

Article

Fluid Identification Method of Nuclear Magnetic Resonance and Array Acoustic Logging for Complex Oil and Water Layers in Tight Sandstone Reservoir

Ze Bai ^{1,2} , Maojin Tan ^{2,*}, Bo Li ², Yujiang Shi ³, Haitao Zhang ³ and Gaoren Li ³

¹ School of Earth and Environment, Anhui University of Science & Technology, Huainan 232001, China; baize@aust.edu.cn

² School of Geophysics and Information Technology, China University of Geosciences, Beijing 100083, China; libocugb@email.cugb.edu.cn

³ Research Institute of Exploration and Development, PetroChina Changqing Oilfield Company, Xi'an 710018, China; syj_cq@petrochina.com.cn (Y.S.); zhanght_cq@petrochina.com.cn (H.Z.); lgr2_cq@petrochina.com.cn (G.L.)

* Correspondence: tanmj@cugb.edu.cn

Abstract: In order to improve the logging interpretation accuracy for complex oil and water layers developed in tight sandstone reservoirs, this study takes the Chang 8 member of the Yanchang Formation in the Huanxian area as the research object, and two new fluid identification methods were constructed based on nuclear magnetic resonance (NMR) logging and array acoustic logging. Firstly, the reservoir characteristics of physical properties and conductivity were studied in the research area, and the limitations of conventional logging methods in identifying complex oil and water layers were clarified. Then, the sensitive parameters for identifying different pore fluids were established by analyzing the relationship between NMR logging and array acoustic logging with different pore fluids. On this basis, the fluid identification plate, composed of movable fluid apparent diffusion coefficient and effective porosity difference ($D_a - \Delta\phi_e$) by NMR logging data of D9TWE3 observation mode, and the other fluid identification plate, composed of apparent bulk modulus of pore fluid and elastic parameter sensitive factor (K_f -Fac), were constructed, respectively. Finally, these two fluid identification methods were used for reservoir interpretation of actual logging data. This study shows that the two new fluid identification methods constructed by NMR logging and array acoustic logging can effectively eliminate the interference of rock skeleton on logging interpretation, which make them more effective in identifying complex oil and water layers than the conventional logging method. Additionally, the two methods have their own advantages and disadvantages when used separately for interpreting complex oil and water layers, and the comprehensive interpretation of the two methods provides a technical development direction for further improving the accuracy of logging the interpretation of complex oil and water layers.

Keywords: tight sandstone; complex oil and water layers; nuclear magnetic resonance logging; array acoustic logging; fluid identification



Citation: Bai, Z.; Tan, M.; Li, B.; Shi, Y.; Zhang, H.; Li, G. Fluid Identification Method of Nuclear Magnetic Resonance and Array Acoustic Logging for Complex Oil and Water Layers in Tight Sandstone Reservoir. *Processes* **2023**, *11*, 3051. <https://doi.org/10.3390/pr11113051>

Academic Editors: Carlos Sierra Fernández and Qingbang Meng

Received: 18 September 2023

Revised: 13 October 2023

Accepted: 18 October 2023

Published: 24 October 2023



Copyright: © 2023 by the authors. Licensee MDPI, Basel, Switzerland. This article is an open access article distributed under the terms and conditions of the Creative Commons Attribution (CC BY) license (<https://creativecommons.org/licenses/by/4.0/>).

1. Introduction

With exploration and development continually being undertaken, the reservoirs with low porosity and low permeability represented by tight sandstone have become a promising exploration and development target for hydrocarbon reserves [1–3]. However, the complex interplay between depositional and post-depositional “diagenetic” attributes obliterates the petrophysical characteristics of sandstone reservoirs resulting in a tight pore. Combined with the influence of logging conditions and reservoir factors, the sensitivity of the logging response to pore fluid is reduced and complex oil and water layers, such as high-resistivity water layers and low-resistivity oil layers, are often misjudged or missed, which seriously

restricts the economic benefits of the oilfield [4–6]. Nowadays, the research on the fluid identification method of complex oil and water layers in tight sandstone reservoirs has become an important topic in oilfield exploration and development [7–10].

Due to the limitation of the measurement mode, the response of conventional logging is seriously affected by rock skeleton, which makes it difficult to identify pore fluid types by using conventional logging methods in tight sandstone reservoirs [11,12]. Additionally, the complex interactions between sedimentation and diagenesis in tight sandstone reservoirs result in strong heterogeneity in the pore structure, and there are significant differences in logging responses for the same pore fluid type [13,14]. In recent years, the newly developed non-electrical logging technology represented by nuclear magnetic resonance (NMR) logging and array acoustic logging is considered to be a powerful tool in dealing with the logging interpretation problems of tight sandstone reservoirs [15,16]. In terms of fluid identification of NMR logging, the most commonly used methods of fluid identification using one-dimensional NMR logging data mainly include two types: the first type includes the difference spectrum method (DSM) and time domain analysis method (TDA) based on the double TW observation mode, which are mainly used to identify light hydrocarbons and water; the second type includes the shift spectrum method (SSM) and enhanced diffusion method (EDM) based on the double TE observation mode, which are mainly used to identify heavy oil and water [17,18]. However, since the nuclear magnetic T_2 spectrum is easily affected by pore structure, fluid distribution in micropores, and fluid types, some logging interpretation methods developed based on NMR logging are not applicable in tight reservoirs [19,20]. Although the two-dimensional NMR logging includes more comprehensive information and has more advantages in fluid identification of tight sandstone reservoirs than one-dimensional NMR logging, it has not been widely used in many oilfields because of its high price and complex data processing process [21–23]. In terms of fluid identification by array acoustic logging, array acoustic logging can directly measure the P-wave velocity and S-wave velocity of reservoir rock and can calculate the elastic parameters reflecting the comprehensive properties of skeleton and pore fluid. When the rock is full of different fluids, the values of elastic parameters are also different, which is the theoretical basis of fluid identification by array acoustic logging [24–26]. Array acoustic logging has great advantages in the identification of gas reservoirs. For oil reservoirs, due to the small difference in elastic parameters between oil and water compared with gas reservoirs, coupled with the influence of rock skeleton, this technology is not widely used in the identification of oil reservoirs, especially tight oil reservoirs [27–29]. It can be seen that, although NMR and array acoustic logging have great advantages during the interpretation of tight sandstone reservoirs, the existing fluid identification methods are still influenced by reservoir pore structures and rock skeleton. And it is necessary to construct more effective logging interpretation methods by deeply analyzing the relationship between different pore fluids and logging responses in tight sandstone reservoirs.

In this research, the Chang 8 tight sandstone reservoir of the Yanchang Formation in the Huanxian area was taken as the research object. The sensitive parameters for identifying different pore fluids were studied and established by analyzing the relationship between NMR logging and array acoustic logging with different pore fluids. And two new fluid identification methods were constructed for interpreting complex oil and water layers, which could eliminate the interference of rock skeleton and pore structures on logging interpretation. The application results illustrate the effectiveness of the two methods to interpret complex oil and water layers in the study area, which can provide a certain significant reference for oil exploration and development in other similar areas.

2. Geologic Setting of the Study Area

The Huanxian area is located in the southwest of the Ordos Basin. The regional structure spans the two geological structural units of the Tianhuan depression and the Yishan slope. It is a superimposed development area of two oil-bearing groups including the Triassic Yanchang Formation and the Jurassic Yan'an Formation (Figure 1). The main

target bed of this study is the Chang 8 tight sandstone reservoir of the Yanchang Formation, which is located below the Chang 7 oil shale and it is the main production horizon of oil and gas because of its good hydrocarbon storage conditions [30,31].

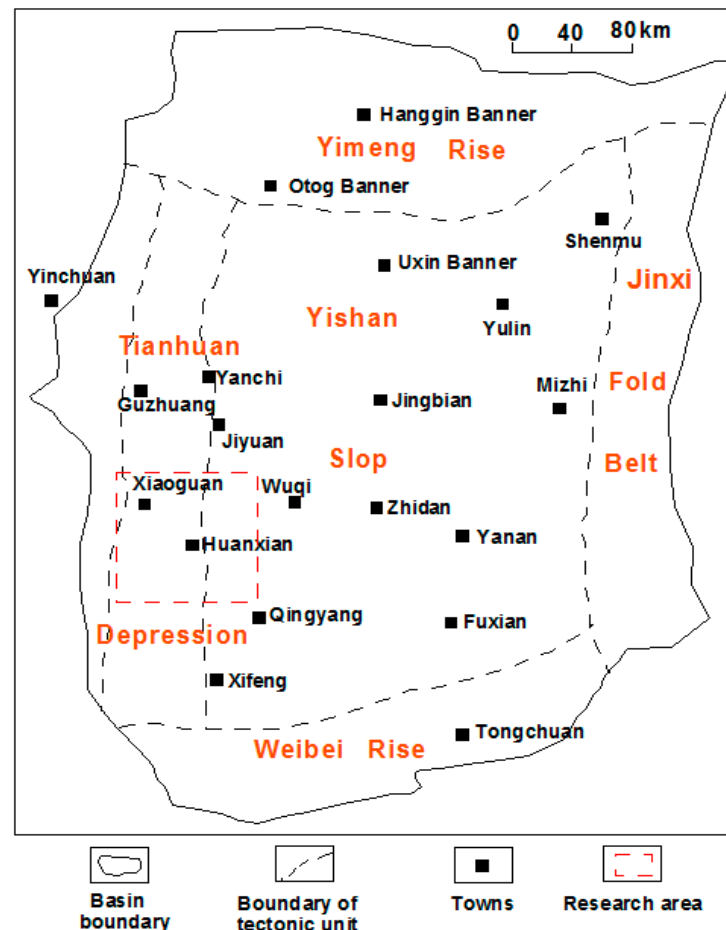


Figure 1. The location map of study area.

The geological conditions of the Chang 8 reservoir of the Yanchang Formation are complex. It is mainly fine sandstone deposited by underwater distributary channels and the deposition thickness of the sand body is large, about 80 m to 100 m. There is strong heterogeneity of the sand body structure, large changes in porosity and permeability properties, and a good exponential relationship is satisfied between porosity and permeability. The main distribution range of porosity is 4.0~10.0%, with an average value of 7.2%. The main distribution range of permeability is 0.01~0.3 md, with an average value of 0.21 md. This is typical of a low-porosity and low-permeability reservoir (Figure 2).

The crossplot of reservoir density (DEN) and resistivity (RT) was drawn to reflect different fluid types' characteristics according to the logging response and oil test conclusion of test intervals (Figure 3). It can be seen that the low-resistivity oil layer, high-resistivity oil layer, and high-resistivity water layer coexist in the study area. The resistivity of the low-resistivity oil layer is distributed between 5 $\Omega \cdot m$ ~10 $\Omega \cdot m$ and the resistivity of the high-resistivity water layer is distributed between 10 $\Omega \cdot m$ ~20 $\Omega \cdot m$. With the increase in reservoir density, the resistivity logging value increases. The density of the low-resistivity oil layer is low and its physical properties are slightly better, which make it difficult to distinguish from the low-resistivity water layer. The high-resistivity water layer and the high-resistivity oil layer have a high density and relatively poor physical properties, and they are also difficult to distinguish from each other. The fluid identification method based

on conventional resistivity logging and porosity logging is not suitable for the interpretation of complex oil and water layers in tight sandstone reservoirs.

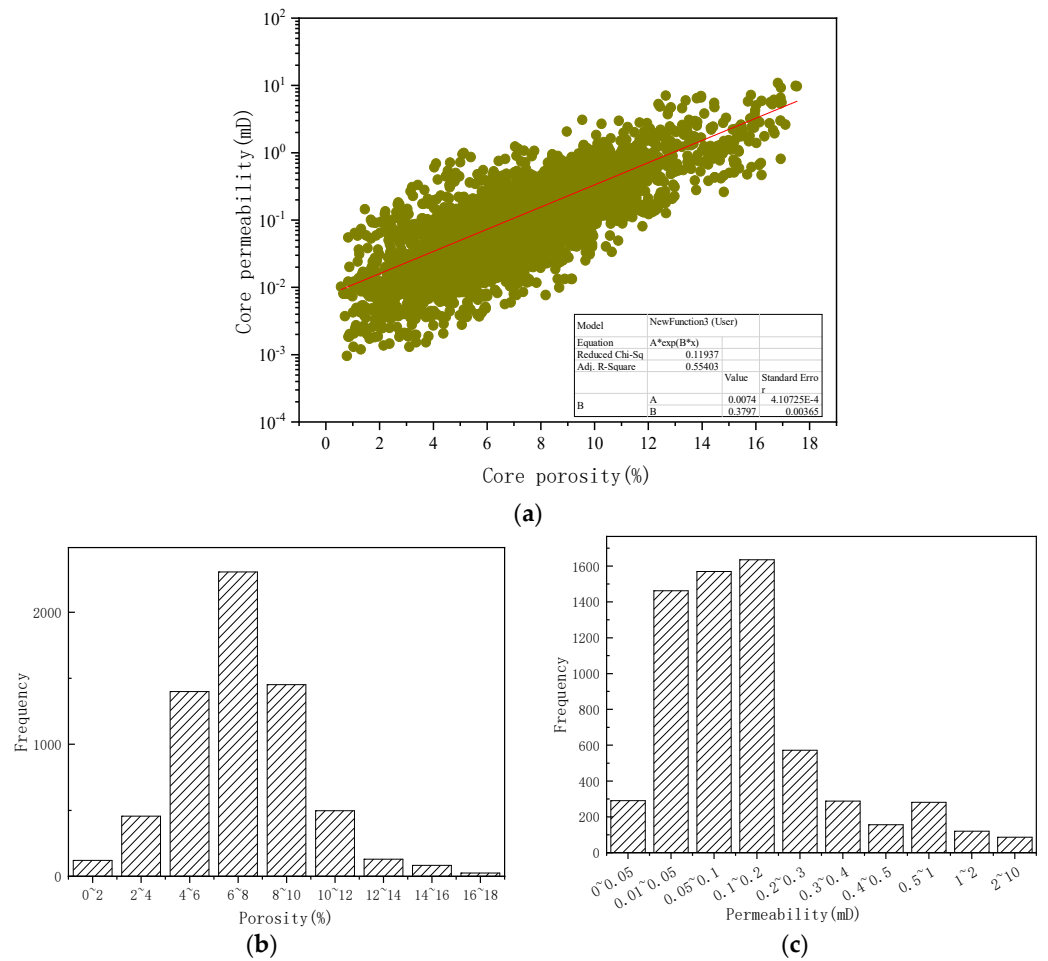


Figure 2. The characteristics of reservoir porosity and permeability. (a) The relationship between porosity and permeability. (b) Reservoir porosity distribution histogram. (c) Reservoir permeability distribution histogram.

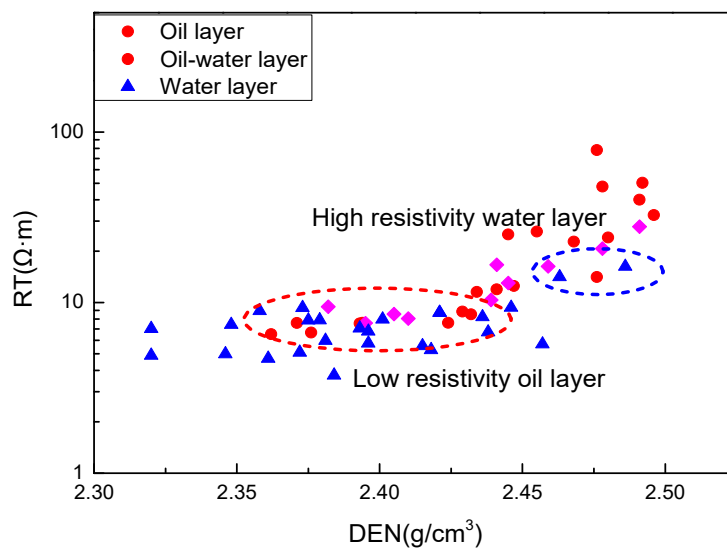


Figure 3. Density and resistivity crossplot of reservoir with different fluids.

3. Data and Methods

3.1. NMR Logging

NMR logging is used to interpret and evaluate the reservoir by measuring the relaxation signal of hydrogen atoms in the formation pore fluid, which can directly reflect the relevant characteristics of fluid types. Different fluids in rock pores have different NMR properties. These fluids can be effectively identified by designing different observation modes.

According to the NMR relaxation mechanism of porous media rocks, the transverse relaxation time is the comprehensive contribution of three relaxation mechanisms, namely, pore fluid free relaxation, surface relaxation, and diffusion relaxation, which can be expressed as the following relationship:

$$\frac{1}{T_2} = \frac{1}{T_{2B}} + \rho_2 \frac{S}{V} + \frac{D(\gamma GT_E)^2}{12} \quad (1)$$

where T_{2B} is the transverse relaxation time of the volumetric fluid, ms, and ρ_2 represents the surface relaxation characteristics of rock particles that are non-dimensional, which depends on the mineral composition of the surface and the properties of hydrocarbon containing fluid in pores. S and V represent the surface area and volume of pores, respectively. D is the diffusion coefficient of pore fluid, cm^2/ms . γ represents the spin magnetic ratio coefficient of the hydrogen atom, $\text{rad}/(\text{s}\cdot\text{T})$. For the hydrogen nucleus, $\gamma = 2.6751 \times 10^8 \text{ rad}/(\text{s}\cdot\text{T})$; G is the magnetic field gradient, generally taking the constant gradient field $G = 20 \text{ Gs}/\text{cm}$. T_E is the echo interval, ms.

At present, NMR logging mainly uses the difference spectrum method (DSM) and shift spectrum method (SSM) for fluid identification. The theoretical basis of the two methods is that there are differences in the transverse relaxation time of pore fluid under different waiting times (double TW) or different echo intervals (double TE). However, the characteristics of the T_2 spectrum will be affected by the reservoir pore structure, pore fluid properties, and rock wettability, especially for tight sandstone reservoirs. The influence of these factors can not be underestimated, resulting in the reduction in fluid identification ability of DSM and SSM. The diffusion coefficient of fluid (D) in Formula (1) is a parameter directly related to the pore fluid types, and the D of different fluid types is different. Among them, the diffusion coefficient of water (D_w) is only affected by temperature, the diffusion coefficient of oil (D_o) is related to viscosity and temperature, and the diffusion coefficient of gas (D_g) is related to density and temperature [32]. The calculation formula is as follows:

$$\begin{aligned} D_o &= \frac{C(T+273.15)}{298\mu} \\ D_w &= 1.0413 + 0.03928T + 0.00040318T^2 \\ D_g &= 0.085 \frac{(T+273.15)^{0.9}}{\rho} \end{aligned} \quad (2)$$

where C is a constant, usually about 1.4, non-dimensional; T is the temperature, $^\circ\text{C}$; μ represents viscosity, $\text{mPa}\cdot\text{s}$; and ρ is the density, g/cm^3 . Based on Formula (2), it can be calculated that the diffusion coefficient of formation water is about 10 times that of formation crude oil at the same depth. Therefore, if the apparent diffusion coefficient of pore fluid (D_a) can be inversely calculated based on NMR logging, the influence of reservoir pore structure and wettability on fluid identification can be effectively avoided.

Assuming that the formation fluid is a single-phase fluid, for the measurement model of double TE, Formula (1) can be written into the following two equations:

$$\begin{aligned} \frac{1}{T_{2s}} &= \frac{1}{T_{2int}} + \frac{D(\gamma GT_{Es})^2}{12} \\ \frac{1}{T_{2L}} &= \frac{1}{T_{2int}} + \frac{D(\gamma GT_{EL})^2}{12} \end{aligned} \quad (3)$$

where T_{2L} and T_{2s} are the lateral relaxation time retrieved at long waiting time and long echo interval, and long waiting time and short echo interval, respectively; T_{2int} is the

inherent relaxation time of rock, ms; T_{ES} and T_{EL} represent short echo interval and long echo interval, respectively, here $T_{ES} = 0.9$ ms and $T_{EL} = 3.6$ ms. The original data of NMR logging are a series of echo strings reflecting the hydrogen atom signal of pore fluid. These echo signals are the overall response of various relaxation components in the pore and the expression is:

$$E_{CHO}(t) = \sum_{i=1}^m P_i e^{-\frac{t}{T_{2i}}} \quad (4)$$

where P_i is the proportion of characteristic relaxation; T_{2i} is the transverse characteristic relaxation time; and m is the divided groups of T_2 . And the calculation process of P_i based on Formula (4) is called T_2 spectral inversion. The inversed T_2 spectrum includes both bound fluid volume signal and movable fluid volume signal. For logging interpretation, bound fluid is considered to be immovable, and the calculated movable fluid volume signal is more meaningful. In order to determine a fixed and effective T_2 cut-off value in our study area, 34 representative cores were selected for NMR experiment, and then the average value of the T_2 cut-off values is taken as the limit value of T_2 spectrum movable fluid volume signal inversion of NMR logging, that is, the inversion starts from the echo string signal behind the T_2 cut-off value, and the inversed T_2 spectrum information is considered as movable fluid information. Figure 4 shows the T_2 distribution of an NMR experiment of 34 cores. Table 1 shows the calculation parameters of the NMR experiment of 34 corresponding cores, in which the average value of the T_2 cut-off value is 9.95 ms and 10 ms was chosen as the T_2 cut-off value in this research (see the red dashed line in Figure 4).

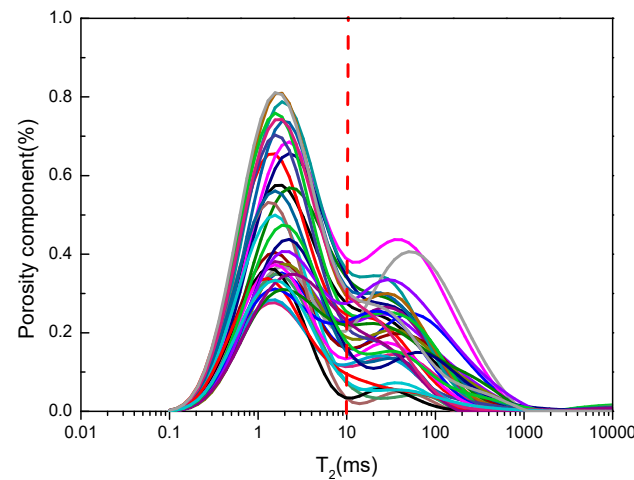


Figure 4. T_2 distribution of core NMR experiment (total 34 cores and the main frequency of the experimental instrument is 2 MHz).

Based on Formula (3), it can be seen that to solve the D_a of movable fluid, it is necessary to find a one-dimensional eigenvalue that can represent the transverse relaxation time. In this paper, the geometric mean value of T_2 is used to represent the inverted T_2 spectrum, that is, Formula (3) can be expressed as follows:

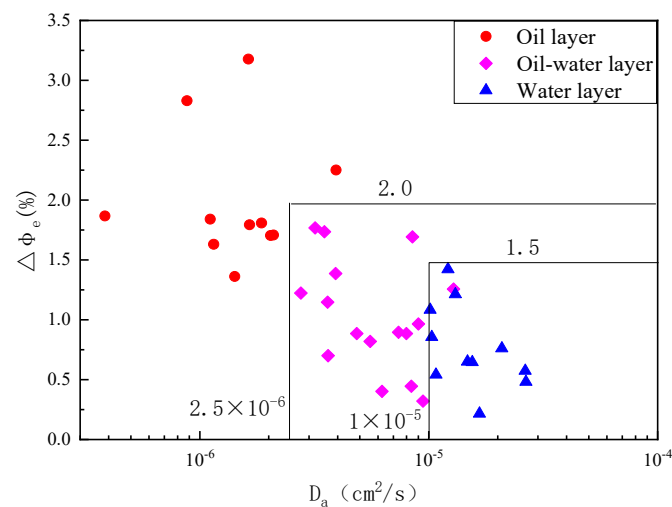
$$\begin{aligned} \frac{1}{T_{2LMSS}} &= \frac{1}{T_{2int}} + \frac{D_a(\gamma G T_{ES})^2}{12} \\ \frac{1}{T_{2LMSL}} &= \frac{1}{T_{int}} + \frac{D_a(\gamma G T_{EL})^2}{12} \end{aligned} \quad (5)$$

where T_{2LMSS} and T_{2LMSL} are the T_2 geometric mean values of movable fluid retrieved from long waiting time and short echo interval, and long waiting time and long echo interval, respectively. T_{2int} represents the characteristic value of the inherent relaxation time of the rock. Thus, D_a and T_{2int} can be obtained by solving Equation (5).

Table 1. Calculation parameters of core NMR experiment.

Num. of Cores	Porosity (%)	S_{wb} (%)	S_{wf} (%)	T_2 Cut-Off Value (ms)	Num. of Cores	Porosity (%)	S_{wb} (%)	S_{wf} (%)	T_2 Cut-Off Value (ms)
B4-4	5.41	92.29	7.71	33	M159-4	8.17	68.12	31.88	4.05
B4-8	13.37	85.25	14.75	4.08	Z488-1	7.56	74.29	25.71	2.96
M131-4	6.55	95.26	4.74	15.13	L296-1	2.55	94.05	5.95	8.432
M165-3	7.08	93.05	6.95	33	L296-3	11.54	92.65	7.35	2.05
M165-7	13.91	86.48	13.52	12.34	C30-3	4.19	53.39	46.61	20.21
M165-8	14.19	85.53	14.47	6.57	B20-4	5.4	66.96	33.04	4.47
M45-7	11.36	89.71	10.29	2.15	H82-6	7.13	78.74	21.26	3.39
H12-2	4.84	94.04	5.96	9.61	Z491-2	8.86	79.02	20.98	3.03
H12-3	13.89	92.52	7.48	4.07	Z491-3	11.6	60.23	39.77	2.79
H12-6	4.82	93.09	6.91	33	L129-2	9.83	69.86	30.14	2.48
M116-2	13.16	84.03	15.97	3.85	H11-1	11.99	83.43	16.57	33
M116-5	11.15	91.86	8.14	3.2	L339-3	5.87	63.7	36.3	6.64
M116-6	10.49	81.86	18.14	17.59	L339-1	14.01	64.09	35.91	11.82
M132-6	15.24	73.15	26.85	5.2	L144-2	1.23	89.75	10.25	6.25
M132-7	8.19	75.7	24.3	9.27	L144-3	8.59	90.31	9.69	3.68
Z318-2	12.5	84.46	15.54	2.7	L215-1	8.1	84.32	15.68	2.18
L253-6	5	80.11	19.89	21.31	Z278-2	8.52	80.71	19.29	4.78

Take the D_a calculated by NMR double TE data as the first fluid identification factor and the effective porosity difference ($\Delta\phi_e$) calculated by double TW data as the second fluid identification factor. Figure 5 is the constructed fluid identification plate (D_a - $\Delta\phi_e$) by comprehensively using double TW and double TE NMR logging data in the study area. It can be seen that the oil layer, oil-water layer, and water layer can be well separated by using D_a - $\Delta\phi_e$. The limit value of D_a between the oil layer and oil-water layer is 2.5×10^{-6} cm²/s, and the limit value of D_a between the oil-water layer and water layer is 1×10^{-5} cm²/s. The limit value of $\Delta\phi_e$ is about 1.5 between the water layer and oil-water layer, and the limit value of $\Delta\phi_e$ is about 2.0 between the oil layer and oil-water layer.

**Figure 5.** The fluid identification plate of NMR logging.

3.2. Array Acoustic Logging

The theoretical basis of fluid identification by array acoustic logging is that when different types of fluids are contained in rock pores, the elastic parameters of rock are different. Therefore, the fluid types can be identified by analyzing the abnormal changes of elastic parameters calculated by array acoustic logging.

It is considered that the bulk modulus of water in the formation is about twice that of oil. As long as the water in the formation pores is replaced by oil and gas, the bulk modulus of the formation will decrease. However, due to the influence of rock skeleton, this difference is sometimes not obvious. If the bulk modulus of formation pore fluid can be calculated by array acoustic logging data, the oil and water layers can be determined more effectively. The formula for calculating the formation bulk modulus by using the acoustic velocity is:

$$K_s = \rho_b (V_p^2 - \frac{4}{3}V_s^2) \quad (6)$$

where V_p and V_s are P-wave velocity and S-wave velocity, respectively, m/s; ρ_b is the bulk density logging response, g/cm³; and K_s represents the rock bulk modulus, GPa. According to the fluid substitution theory of the Gassmann equation, the bulk modulus of rock can also be expressed as follows:

$$K_s = K_d + \frac{(1 - \frac{K_d}{K_m})^2}{\frac{\phi}{K_f} + \frac{1-\phi}{K_m} + \frac{K_d}{K_m^2}} \quad (7)$$

where K_s represents the bulk modulus of saturated rock; K_f represents the bulk modulus of rock pore fluid; K_d represents the bulk modulus of dry rock, which is related to the modulus and pore characteristics of rock skeleton; K_m represents the bulk modulus of rock skeleton; and ϕ represents reservoir porosity, decimal. Based on Formula (7), the expression of apparent bulk modulus (K_{fa}) of pore fluid can be deduced as follows:

$$K_{fa} = \frac{1}{\phi} \left(\frac{(1 - \frac{K_d}{K_m})^2}{K_s - K_d} - \frac{K_d}{K_m^2} - \frac{1 - \phi}{K_m} \right) \quad (8)$$

The K_s can be obtained by using Equation (6). In order to calculate K_{fa} , K_d and K_m also need to be determined. Keys and Xu (2002) proposed the calculation method of K_d based on the Xu–White model and K_d can be written as follows [33]:

$$K_d = K_m(1 - \phi)^P \quad (9)$$

where P is the pore aspect ratio function, which is related to the uniform strain field and ellipsoidal pore strain field at infinity. The skeleton modulus of rock can be calculated by using the Voigt–Reuss–Hill model. Assuming that the reservoir rock is sandy mudstone stratum, the elastic modulus of rock skeleton can be expressed as follows:

$$\begin{aligned} M_V &= \frac{V_c}{1-\phi} M_c + \frac{1-V_c-\phi}{1-\phi} M_s \\ \frac{1}{M_R} &= \frac{V_c}{1-\phi} \frac{1}{M_c} + \frac{1-V_c-\phi}{1-\phi} \frac{1}{M_s} \\ M_m &= \frac{M_V + M_R}{2} \end{aligned} \quad (10)$$

where M_v and M_R are Voigt upper bound and Reuss lower bound, respectively. M_c and M_s represent the elastic modulus of mudstone and sandstone skeleton, respectively. V_c represents the shale content in the rock skeleton, which can be calculated by natural gamma logging (GR). M_m represents the elastic modulus of rock skeleton. Sun et al. (2016) gave the specific values of elastic parameters and pore aspect ratio of different rock components during the analysis of the tight sandstone reservoir in the Ordos Basin (Table 2) [34].

Thus, K_{fa} can be calculated by substituting these parameters and calculation results into Formula (7).

Table 2. Elastic parameters and pore aspect ratio of different rock components.

Rock Components	Bulk Modulus (GPa)	Shear Modulus (GPa)	Pore Aspect Ratio
Shale	27.3	17.6	0.013
Sand	37.0	44.0	0.14
Salt water	2.2	0	/
Oil	1.0	0	/
Gas	0.05	0	/

In order to determine the second sensitive elastic parameter, it is assumed that the average shale content of the reservoir rock is 15%, and then the variation characteristics of Poisson's ratio and lame constant with porosity when the rock is filled with different fluids are simulated by the Gassmann equation, as shown in Figure 6. It can be seen that when the rock pore is saturated with natural gas, Poisson's ratio and lame constant are the smallest, followed by saturated oil, and the largest when saturated with salt water. With the increase in porosity, Poisson's ratio gradually increases and the lame constant gradually decreases. Therefore, the division of lame constant and Poisson's ratio is considered as the second sensitive elastic parameter, that is $Fac = \frac{\lambda}{\sigma}$.

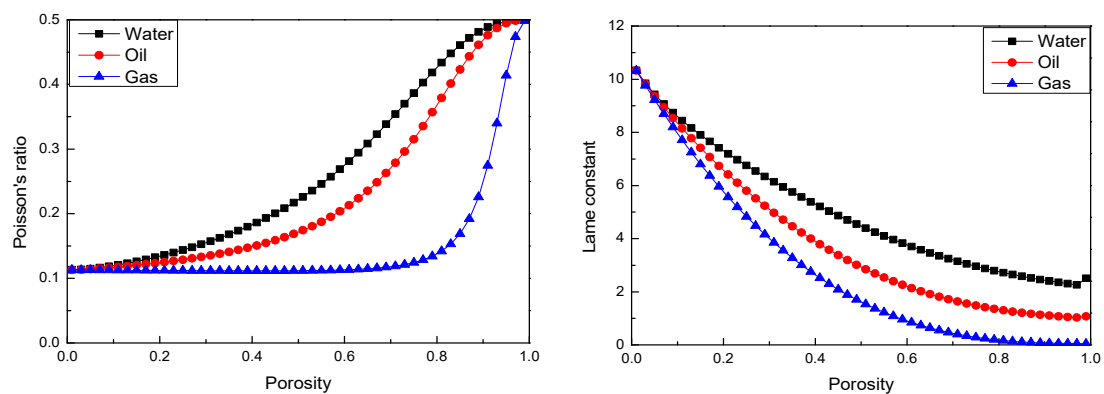


Figure 6. Relationship between different elastic parameters and porosity when rocks are saturated with different fluids.

According to the relationship between density and resistivity among different fluid types in the study area (Figure 3), the high-resistivity oil layer has a higher density and relatively smaller porosity than the low-resistivity oil layer. And the calculated lame constant should be higher and Poisson's ratio should be lower in the high-resistivity oil layer than in the low-resistivity oil layer. Therefore, the high-resistivity oil layer should have a high Fac value and low K_{fa} value. The low-resistivity oil layer has a low Fac value and low K_{fa} value. The water layer has a low density and its porosity is good, but the oil saturation is low, so the Fac value is small and the K_{fa} value is large. Figure 7 shows the fluid identification plate constructed by using array acoustic logging data of 12 wells in the study area. It can be seen that the boundary of different fluids is relatively clear, indicating that this method can be used to carry out fluid identification.

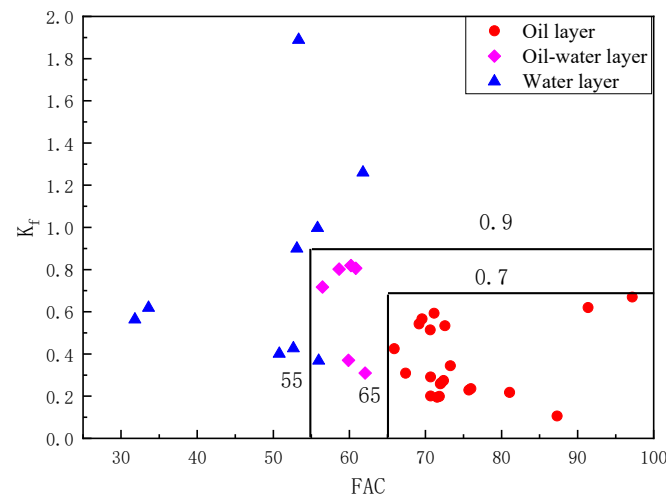


Figure 7. The fluid identification plate of array acoustic logging.

4. Application Results Analysis

The proposed fluid identification method was applied to interpret the six array acoustic logging data and five D9TWE3 observation mode NMR logging data in the study area. The interpretation results are shown in Table 3. It can be seen that five horizons in the fluid identification results of six array acoustic logging data were correctly interpreted, of which three horizons are low-resistivity oil reservoirs (well L351, well L350, and well L184). The oil test result of another layer is water layer, but it is interpreted as the oil–water layer (well M132). The resistivity and density logging values of this layer are $15.54 \Omega \cdot \text{m}$ and 2.49 g/cm^3 , respectively, and it is a high-resistivity water layer, which indicates that the fluid identification plate established by the array acoustic wave has a weaker identification effect on the high-resistivity water layer with poor physical properties, but a better identification effect on the low-resistivity oil layer. Among the five NMR logging fluid identification results, four horizons were correctly interpreted, and the oil test result of the other one is an oil–water layer, but they are interpreted as oil layers, which shows that the NMR logging fluid identification method has a relatively poor effect on distinguishing between oil layers and oil–water layers. On the whole, the application effect of these two fluid identification methods in the study area is good.

Table 3. Comparison of fluid identification effects.

Method	Well	Interpretation Interval (m)	Resistivity ($\Omega \cdot \text{m}$)	Density (g/cm^3)	X-Axis Fluid Identification Factor	Y-Axis Fluid Identification Factor	Interpretation Results	Testing Results	
								Oil (t/d)	Water (m^3/d)
Array acoustic logging	L351	2531–2534	15.34	2.41	72.098	0.274	Oil	6.46	0
	L350	2672–2678	7.89	2.38	73.271	0.344	Oil	31.28	0
	L252	2360–2368	33.67	2.39	77.770	0.309	Oil	15.3	0
	L184	2233–2238	10.98	2.42	68.796	0.581	Oil	10.1	0
	M87	2652–2659	17.62	2.40	59.876	0.371	Oil–water	4.42	13.1
	M132	2647–2655	15.54	2.49	56.564	0.717	Oil–water	0	19.7
NMR logging	L89	1967–1971	11.08	2.43	1.11×10^{-6}	1.839	Oil	21.25	0
	B236	2582–2591	21.16	2.45	2.04×10^{-6}	1.701	Oil	9.35	7.8
	Y111	2688–2694	14.96	2.48	1.28×10^{-5}	0.694	Water	0	6.9
	L100	2503–2506	17.59	2.49	1.31×10^{-5}	1.452	Water	0	12.5
	B286	2679–2690	7.25	2.44	2.66×10^{-5}	0.472	Water	0	9.8

In order to further illustrate the application effect of the fluid identification method constructed by NMR logging and array acoustic logging, the interpretation results were compared with the conventional interpretation results. Figure 8 is an interpretation example of well Y111 by using NMR logging. In Figure 8, the fifth track is the T_2 spectrum distribution characteristics inverted by the long waiting time and short echo interval signals (TASPEC). The sixth track is the T_2 spectrum distribution characteristics inverted by the long waiting time and long echo interval signals (TDSPEC). The seventh track is the signal inverted by the difference spectrum of different waiting time (DSTW), and the eighth track is the effective porosity difference ($\Delta\phi_e$) calculated by the different waiting time. Curves BASEY1 and BASEY2 are the two limit values 1.5 and 2.0 of the effective porosity difference in the fluid identification plate, respectively. The ninth track is the apparent diffusion coefficient (D_a) of the movable fluid calculated by using the data of different echo intervals. The curves BASEX1 and BASEX2 are the limit value $1 \times 10^{-5} \text{ cm}^2/\text{s}$ and $2.5 \times 10^{-6} \text{ cm}^2/\text{s}$ of the D_a in the fluid identification plate, respectively. It can be seen that from 2688.5 m to 2694.875 m of the reservoir section, the resistivity logging curves of different detection depths are almost overlapped. The value of deep induction resistivity is relatively high, with an average of $14.96 \Omega\cdot\text{m}$. There are signals in the double TW difference spectrum. The original logging interpretation conclusion is that this layer is the oil–water layer. However, the calculated D_a value is basically greater than 1×10^{-5} and $\Delta\phi_e$ less than 1.5. According to the proposed fluid identification method by NMR logging, this layer was ultimately interpreted as a water layer. Then, the oil testing was carried out in the interval of 2690.2 m to 2691.8 m, and the testing result is 6.9 m^3 per day of water production with no oil coming out, indicating that it is a high-resistivity water layer, which further confirms the accuracy of our interpretation results.

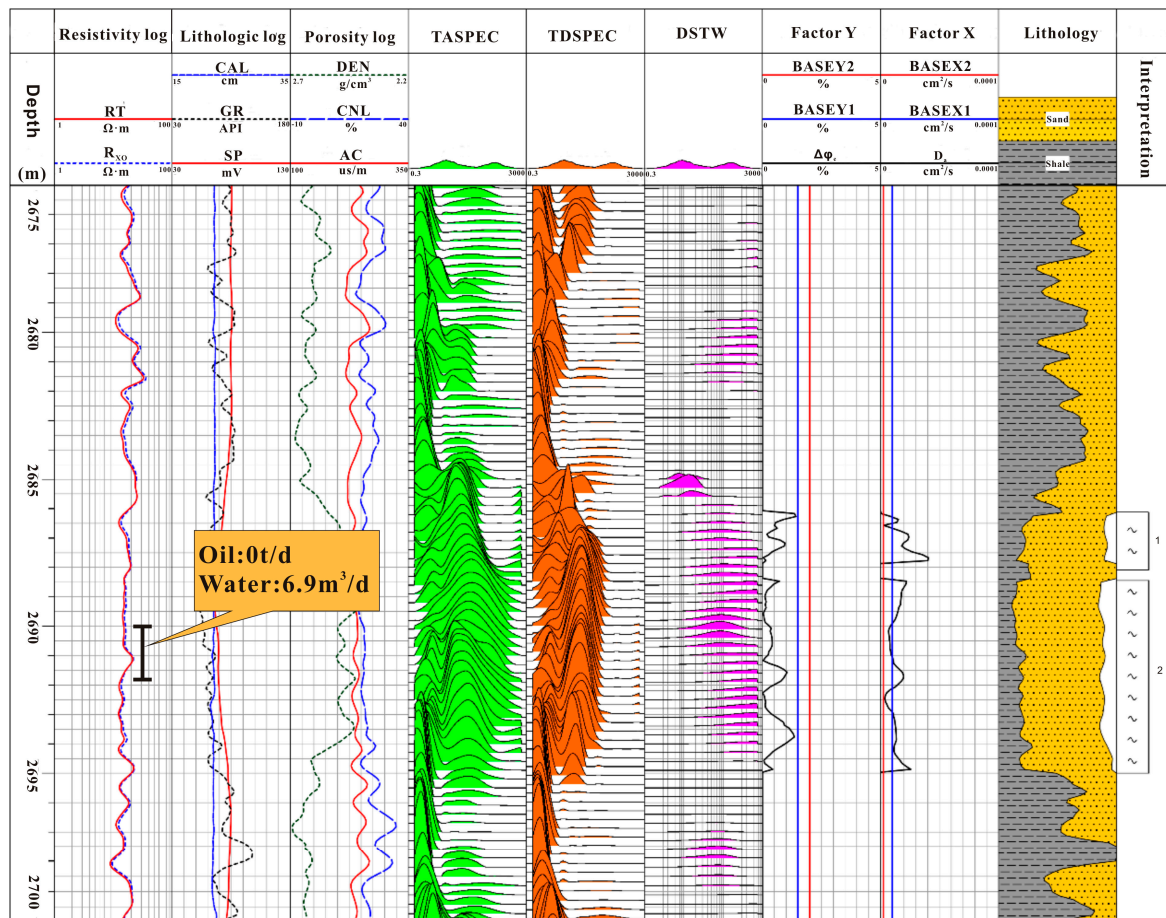


Figure 8. The application results of NMR logging fluid identification method (well Y111).

L184 is a key evaluation well in the study area using array acoustic logging. Figure 9 shows the interpretation results by using the proposed fluid identification plate of array acoustic logging. The fifth track in the figure is the elastic parameter calculated by array acoustic logging. The sixth track is the result of overlapping the apparent P-wave curve of 100% water bearing formation (MDTS) calculated by array acoustic logging and the measured P-wave curve (DTCQI). Based on the P-wave curve overlap method, it is generally believed that the larger the overlapping difference area between MDTS and DTCQI, the better the oil content of the reservoir [35]. The eighth track is the fluid identification indication curve according to the limit values of the array acoustic logging fluid identification plate. In the fluid identification indication curve, the number “2” represents the oil layer, the number “1” represents the oil–water layer, and the number “–2” represents the water layer. By filling the fluid identification indication curve with the 0-value line, the part higher than the 0-value line is filled with red, representing the oil layer, and the part lower than the 0-value line is filled with blue, representing the water layer. It can be seen that from 2232.875 m to 2238.375 m of the reservoir section, the resistivity logging curves at different detection depths show negative differences. The average value of deep induction resistivity logging is 9.04 Ω·m and the P-wave curve overlap method shows that there is a certain difference area in this section. The conventional interpretation method indicates that this section is the oil–water layer, while the fluid indication curve calculated by array acoustic logging shows that this section is a better oil layer. Finally, this layer was interpreted as an oil layer. Then, the oil testing was carried out in the interval of 2233.125 m to 2236 m, and the testing result is 10.1 tons per day of oil production without any water coming out, indicating that it is a low-resistivity oil layer, which confirms the accuracy of our interpretation results.

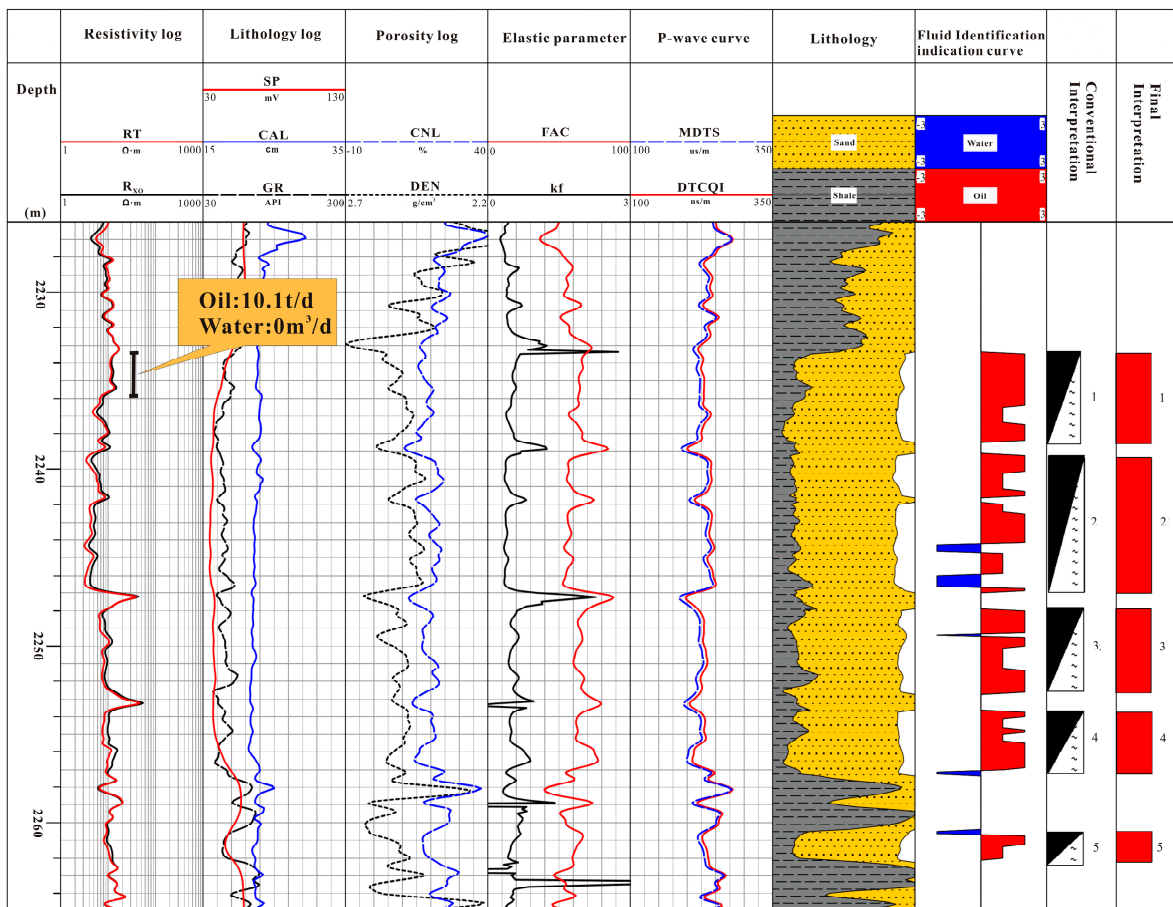


Figure 9. The application results of array acoustic logging fluid identification method (well L184).

The above application results and fluid identification examples show that the fluid identification factors and plates based on NMR logging and array acoustic logging are effective for reservoir fluid identification in the study area. Compared with the conventional interpretation methods, the constructed fluid identification method in this paper has more advantages in the fluid identification of tight sandstone reservoirs.

5. Discussion

NMR logging and array acoustic logging are two commonly used non-electrical logging techniques in oil fields, which can provide rich pore fluid information for tight sandstone reservoirs. Based on the above research, we constructed two fluid identification methods for identifying complex oil and water layers using NMR logging and array acoustic logging, respectively. The construction principle of each fluid identification method is to eliminate the interference of rock skeleton and pore structure on fluid identification as much as possible. Additionally, the good understanding of the properties of different pore fluids in the study area is also crucial for optimizing fluid-sensitive parameters.

The fluid identification factors constructed based on these two non-electrical logging techniques are worthy of affirmation in principle and method, and the constructed fluid identification plates are applicable in the study area. Due to the limitations of logging data in the study area, the two fluid identification methods constructed above are used independently during the actual log interpretation, and there are differences in the application effects of high-resistivity water layers and low-resistivity oil layers of those two methods. It is believed that combining these two methods for comprehensive interpretation can achieve complementary advantages and further improve the accuracy of fluid identification.

6. Conclusions

The Chang 8 member of the Yanchang Formation in the Huanxian area is a typical low-porosity and low-permeability reservoir, with an average porosity and average permeability of 7.2% and 0.21 md, respectively. The strong heterogeneity of reservoir properties results in a weaker sensitivity of the logging response to pore fluids, and the low-resistivity oil layer, high-resistivity oil layer, and high-resistivity water layer coexist in the study area. The complex relationship between pore fluid and logging response makes it difficult to interpret the fluid types by using conventional electrical logging and porosity logging.

To improve the logging interpretation accuracy for complex oil and water layers developed in tight sandstone reservoirs, two new fluid identification methods were constructed by analyzing the sensitive parameters of nuclear magnetic resonance (NMR) logging and array acoustic logging to pore fluids. The NMR logging fluid identification method considers the difference between movable fluid apparent diffusion coefficient (D_a) and effective porosity difference ($\Delta\phi_e$) calculated by dual TW and dual TE data, and the array acoustic logging fluid identification method utilizes the difference between apparent bulk modulus of pore fluid (K_f) and elastic parameter sensitive factor (F_{ac}). These fluid identification factors were obtained through the comprehensive analysis of logging rock physics and reservoir fluid properties in the study area, which effectively eliminated the interference of rock skeleton on logging interpretation. The application results show that the two new fluid identification methods have a better interpretation effect on complex oil and water layers than conventional logging methods. Additionally, the array acoustic logging method is better at identifying low-resistivity oil layers with slightly better physical properties, while the NMR logging method is better at identifying high-resistivity water layers with poorer physical properties, which also provides a direction for future research.

Author Contributions: Conceptualization, M.T.; Methodology, Z.B.; Software, B.L.; Resources, Y.S., H.Z. and G.L.; Writing – original draft, Z.B. All authors have read and agreed to the published version of the manuscript.

Funding: This work is supported by the Natural Science Research Project of the Anhui Educational Committee (Grant No. 2022AH050831), the Anhui Provincial Natural Science Foundation (Grant No. 2208085QD114), and the National Natural Science Foundation of China (Grant No. 42174149).

Data Availability Statement: The data presented in this study are available on request from the corresponding author. The data are not publicly available due to restrictions of privacy.

Conflicts of Interest: The authors declared no conflict of interest.

References

- Gao, J.X.; Sun, W.J.; Wu, P.; Duan, C. Accumulation characteristics of Upper Paleozoic tight sandstone in Shenfu block, northeastern margin of Ordos Basin. *Lithol. Reserv.* **2021**, *33*, 121–130.
- Zhou, L.H.; Chen, C.W.; Han, G.M.; Yang, F. Difference characteristics between continental shale and tight oil and exploration practice: A case from Huanghua Depression, Bohai Bay Basin. *Earth Sci.* **2021**, *46*, 555–571.
- Lu, C.; Li, M.; Guo, J.C.; Zhao, L.; Xu, S.; Chen, B.; Zhou, Y.; Yuan, H.; Tang, Z. Fracture parameters optimization and field application in low-permeability sandstone reservoirs under fracturing flooding conditions. *Processes* **2023**, *11*, 285. [[CrossRef](#)]
- Wen, B.; Zhou, Y. Study on fluid identification of low porosity and low permeability reservoir. *Petrochem. Ind. Technol.* **2017**, *24*, 126.
- Huang, X.H.; Tang, J.R.; Liu, Q.; Ma, Y. Multi-index fusion logging evaluation system for low porosity and low permeability reservoirs. *China Energy Environ. Prot.* **2021**, *43*, 96–102.
- Gao, F.M.; Xiao, L.; Zhang, W.; Cui, W.; Zhang, Z.; Yang, E. Low permeability gas-bearing sandstone reservoirs characterization from geophysical well logging data: A case study of Pinghu formation in KQT region, East China Sea. *Processes* **2023**, *11*, 1030. [[CrossRef](#)]
- Chen, J.; Xie, R.C.; Liu, C.C.; Duan, Y.; Li, H.; Xiang, Y. Logging fluid identification and quantitative evaluation of Jurassic tight sandstone gas reservoir in Zhongjiang gas field. *Nat. Gas Ind.* **2019**, *39*, 136–141.
- Li, C.X.; Liu, M.; Guo, B.C. Classification of tight sandstone reservoir based on NMR logging. *Appl. Geophys.* **2019**, *16*, 549–558. [[CrossRef](#)]
- Wu, P.; Shang, C.H.; Chen, G.H.; Sun, Z.; Jiang, L. Application of EMI in Tight Sandstone Reservoirs of Linxing-Shenfu Block on the Eastern Margin of Ordos. *Well Logging Technol.* **2020**, *44*, 251–255.
- Zhang, X.X.; Zhu, L.F.; Wang, T.J.; Shi, X.; Han, B.; Shen, J.; Gao, H. Fluid property identification of the Lower Cretaceous reservoirs with complex oil-water contacts in Deseo Basin, Chad. *Energy Geosci.* **2023**, *5*, 100219. [[CrossRef](#)]
- Zhang, T.; Zhang, X.G.; Lin, C.Y. Evaluation of pore structure in low permeability reservoirs based on common well logs. *J. Chengdu Univ. Technol.Sci. Technol. Ed.* **2014**, *4*, 413–421.
- Shen, D.; Zhao, J.L. Research and application of logging interpretation method for low resistivity reservoir in Banqiao Oilfield. *Petrochem. Ind. Technol.* **2020**, *27*, 150–151.
- Mahmoud, L.; Andrea, M.; Branimir, S.; Ruffell, A. Depositional facies controls on the diagenesis and reservoir quality of the Messinian Qawasim and Abu Madi formations, onshore Nile Delta, Egypt. *Geol. J.* **2019**, *54*, 1797–1813.
- Mahmoud, L.; Andrea, M.; Dustin, E.S.; Branimir, S. Diagenetic signatures in the deltaic and fluvial-estuarine Messinian sandstone reservoirs in the Nile Delta as a tool for high-resolution stratigraphic correlations. *Int. J. Sedim. Res.* **2023**, *38*, 754–768.
- Zhang, H.T.; Fang, Y.Y.; Li, G.R.; Tan, M.; Wang, X. Nuclear magnetic resonance relaxation mechanism and fluid identification in oil wet tight sandstone reservoirs. *Geophys. Prospect. Pet.* **2020**, *59*, 422–429.
- Lai, F.Q.; Liu, Y.J.; Kou, X.P.; Huang, Z.; Chen, Z.; Liu, Y.; Jiang, G.; Zang, Y.; Wang, M.; Wang, R. Fluid identification based on NMR apparent free water porosity inversion: A case study of Paleozoic tight sandstone gas reservoirs in Western Ordos. *Geofluids* **2022**, *2022*, 2–16. [[CrossRef](#)]
- Hu, F.L.; Zhou, C.C.; Li, C.L.; Xu, H.J.; Zhou, F.M.; Si, Z.W. Water spectrum method of NMR logging for identifying fluids. *Pet. Explor. Dev.* **2016**, *43*, 244–251. [[CrossRef](#)]
- Zhong, J.B.; Yan, R.H.; Zhang, H.T.; Feng, Y.; Li, N.; Liu, X. A decomposition method of nuclear magnetic resonance T₂ spectrum for identifying fluid properties. *Pet. Explor. Dev.* **2020**, *47*, 691–702. [[CrossRef](#)]
- Hamada, N.M.; Al-Blehed, A.S.; Al-Awad, M.N.; Al-Saddique, M.A. Petrophysical evaluation of low-resistivity sandstone reservoir with nuclear magnetic resonance log. *J. Pet. Sci. Eng.* **2001**, *39*, 129–138. [[CrossRef](#)]
- Li, B.; Tan, M.J.; Zhang, H.T. Interpretation method of nuclear magnetic resonance dual-TW logging in oil-wet tight sandstone reservoirs. *Appl. Geophys.* **2020**, *5*, 796–808. [[CrossRef](#)]
- Hu, F.L.; Zhou, C.C.; Li, C.L.; Xu, H.; Zhou, F.; Si, Z. Fluid identification method based on 2D diffusion-relaxation nuclear magnetic resonance (NMR). *Pet. Explor. Dev.* **2012**, *39*, 552–558. [[CrossRef](#)]
- Han, C.; Li, G.; Bie, K.; Yu, D.; Chen, W.; Wu, F. Application of Innovative T₁-T₂ Fluid Typing Method in Complex Carbonate Reservoir of Fengxi Block. *Well Logging Technol.* **2021**, *1*, 56–61.

23. Wang, T.; Zhang, D.D.; Wang, X.; Wang, Z.; Zhang, W.; Sun, W.; Ma, M. Characterization of Movable Fluid Distribution in Tight Oil Reservoirs by NMR and Centrifugation. *Geofluids* **2023**, *2023*, 1668663. [[CrossRef](#)]
24. Shi, W.R.; Wang, X.Z.; Shi, Y.H.; Feng, A.G.; Zou, Y.; Young, S. Application of dipole array acoustic logging in the evaluation of shale gas reservoirs. *Energies* **2019**, *12*, 3882. [[CrossRef](#)]
25. Wang, W.W. Research on Gas Zone Identification in Tight Sand Based on the Fluid Substitution Theory. *Offshore Oil* **2020**, *20*, 57–60.
26. Xing, D.H.; Fan, Y.R.; Lu, H.F.; Lu, C.; Zhang, P.; Li, H.; Ding, Y. A combined method for gas-bearing layer identification in a complex sandstone reservoir. *Front. Earth Sci.* **2022**, *10*, 942895. [[CrossRef](#)]
27. Zhang, L.H.; Pan, B.Z.; Shan, G.Y. Qualitative Identification of Volcanic Reservoir Fluid Property with the Logging Fluid Factor Method. *World Well Logging Technol.* **2015**, *5*, 22–24.
28. Zhang, P.; Yang, Q.Y.; Fan, Y.R.; Zhang, Y.; Zhang, H. Gas-bearing property evaluation of tight sandstone reservoir based on Xu-White model. *Lithol. Reserv.* **2020**, *32*, 138–145.
29. Li, J.C.; He, X.; Zhao, A.S.; Jiang, C. Joint inversion of formation radial shear-velocity profiles by dipole acoustic logging while drilling. *Geophysics* **2023**, *88*, 295–305. [[CrossRef](#)]
30. Wang, C.Y.; Dan, W.D.; Fang, Y.B. The Features and Geological Significance of Shallow Water Delta of Chang 8 Formation in Ordos Basin. *J. Oil Gas Technol.* **2013**, *35*, 12–15.
31. Cui, J.W.; Zhu, R.K.; Luo, Z.; Li, S. Sedimentary and geochemical characteristics of the Triassic Chang 7 member shale in the Southeastern Ordos Basin, Central China. *Pet. Sci.* **2019**, *16*, 285–297. [[CrossRef](#)]
32. Mahmoud, E.; Abubakar, I.; Moaz, H.; Amjed, H.; Karem, A.G.; Mahmoud, M.; El-Husseiny, A.; Radwan, A.E. A review on the applications of nuclear magnetic resonance(NMR) in the oil and gas industry: Laboratory and field-scale measurements. *J. Pet. Explor. Prod. Technol.* **2022**, *12*, 2747–2784.
33. Keys, R.G.; Xu, S. An approximation for the Xu-White velocity model. *Geophysics* **2022**, *39*, 587–618.
34. Sun, J.M.; Wei, X.H.; Chen, X.L. Fluid identification in tight sandstone reservoirs based on a new rock physics model. *J. Geophys. Eng.* **2016**, *13*, 526–535. [[CrossRef](#)]
35. Gu, Y.J. Application of new logging technology in oil-water reservoir evaluation in Lishuao area. *Pet. Geol. Eng.* **2014**, *28*, 44–47.

Disclaimer/Publisher’s Note: The statements, opinions and data contained in all publications are solely those of the individual author(s) and contributor(s) and not of MDPI and/or the editor(s). MDPI and/or the editor(s) disclaim responsibility for any injury to people or property resulting from any ideas, methods, instructions or products referred to in the content.